THE EFFECT OF WAVEGUIDE MATERIAL AND SHAPE ON ACOUSTIC EMISSION TRANSMISSION CHARACTERISTICS
PART 1: TRADITIONAL FEATURES

JOANNA SIKORSKA and JIE PAN
University of Western Australia, Perth, Australia

Abstract

This paper presents the effects of varying waveguide material and/or shape on traditional acoustic emission characteristics of pulsed events. Forty-eight solid cylindrical waveguides were fabricated from alumina ceramic, mild steel, stainless steel (SS316), 2024-T3 aluminium or extruded Delrin. Three different lengths, two diameters and four sensor face angles were tested. The effects of a point at the source end of the waveguide were also verified. Results show that although ceramic guides attenuate the signals more than commonly used grades of steel and aluminium, waveform fidelity is less affected. Points also had a negative effect of all AE features and waveform profiles.

Keywords: acoustic emission testing, waveguides, buffer rods, wave propagation.

1. Relevant Ultrasonic Theory

The solutions to the general wave equation for acoustic waves travelling through infinitely long isotropic cylinders are detailed in references [1-3]. However, there are several key points applicable to this research work that will now be summarised.

Longitudinal (axially symmetric) wave modes in an infinitely long cylinder vary with radial and longitudinal distance along the cylinder but are symmetrical around the circumference. The relationship between longitudinal phase velocity and frequency is known as the Pochammer-Chree equation and resembles the Lamb dispersion relationship in plates. Its solution is well documented and can be found in the aforementioned references.

Group velocities also vary with frequency in a similar fashion. Fig. 1 depicts the first two longitudinal phase and group velocities for one of the materials tested in this study. It can be seen that the fundamental mode approaches a constant speed as frequency approaches zero. This limiting speed corresponds to the longitudinal rod speed, $c_L = \sqrt{E/\rho}$ where E is the Young's modulus for the material and ρ is the density. As frequency increases the first longitudinal modes asymptote to the Rayleigh velocity. Rayleigh waves are surface acoustic waves in which longitudinal and shear modes couple together and travel at a common speed; it is always less than the transverse speed by 5 to 15% [4]. They also decay rapidly with depth and therefore displacements are confined to within one order of Rayleigh wavelengths from the surface. Higher longitudinal modes have cut-off frequencies below which they will not propagate, and above which they are dispersive. Torsional waves (through an infinite cylinder) propagate with one constant phase velocity equal to the shear (or transverse) speed:

$$c_T = \sqrt{\frac{E}{\rho} \cdot \frac{1}{2(1+\nu)}} \qquad (1)$$

where ν is the Poisson's ratio. Again, higher phase modes are dispersive and each has a unique cut-off frequency below which these modes will not propagate as evident in Fig. 2. Cut-off frequencies are a function of the rod diameter (due to the changing velocity), but independent of length. All torsional group velocities are dispersive. Similar, but mathematically more complex relationships govern the dispersive characteristics of flexural (anti-symmetric) waves in rods; these are described in reference [4].

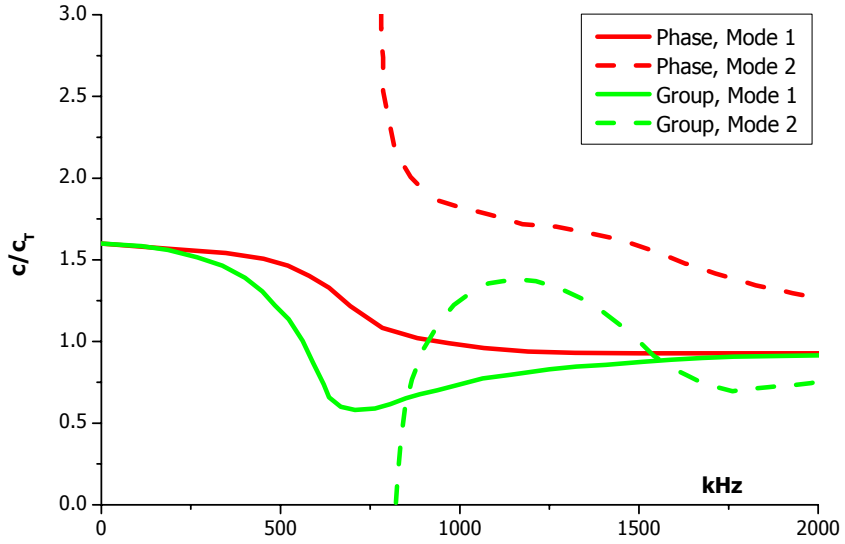

Fig. 1 First two longitudinal modes showing normalised phase and group velocities (latter are shown as dashed lines) for an 8-mm SS316 infinitely long rod waveguide. Wave speed is normalised with respect to transverse wave speed, given in equation (1), whilst frequency is in kHz.

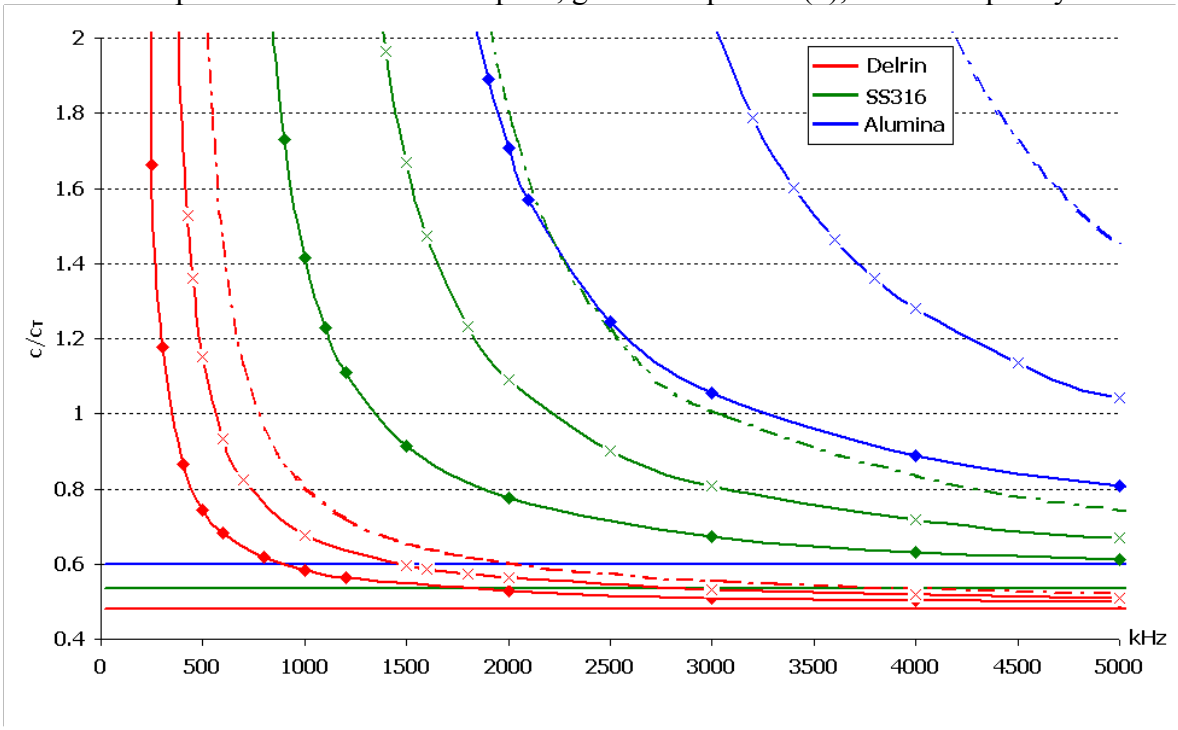

Fig. 2 First four normalised torsional phase velocities for 8-mm diameter, infinitely long waveguides of different materials. Wave speed is normalised with respect to transverse wave speed, given in equation 1, whilst frequency is in kHz.

At very narrow diameters, cut-off effects act like a high pass filter, leaving only lower order modes as the means by which low frequency longitudinal, torsional and flexural waves can be transmitted. Conversely, above a certain frequency, which is a function of rod diameter and material properties (namely E, ρ, and ν) speeds approach their limiting values and dispersion will no longer occur. In this interim region however, where wavelength is in the same order as the rod diameter, significant dispersive effects can be expected.

In addition to dispersion, AE bursts are attenuated as they travel through the material. Some of this energy loss is caused by friction and thermal conductivity and occurs in all materials, independent of frequency. However in compounds with larger grain sizes, such as plastics or composites, frequency-dependant attenuation can increase significantly (by up to 3 orders of magnitude). Attenuation is also generally greater for transverse waves than for longitudinal modes. Finally, it is important to recognise that AE sensors are not equally sensitive to all wave modes, causing further apparent signal reduction of various modes.

One side effect of dispersion is the tendency of AE bursts, which are made up of numerous waves of different polarizations and consequently different speeds, to lengthen in time as they move further from the source. Called *mode separation*, continuous transformation between modes exacerbates this effect [5].

In a finite rod, wave motion becomes even more complicated due to reflections from, and resonance at, both ends [6]. Acoustic waves are partially reflected and transmitted at every interface, the relative amounts of which depend on the ratio of the relative characteristic impedances of each pair of boundary materials. This impedance is a function of material density and the speed wave hitting the interface. If material attenuation is low, these reflections will combine with late arriving components of the original signal, thus complicating feature identification.

For non-zero angles of incidence, the character of the wavefront will also change as it hits the interface. Called *mode conversion*, the change in angle of the wavefront will convert part of the incoming wave from longitudinal to shear and vice versa. Flexural waves that may not have been present in the original waveform can also be excited.

Finally, cylinders have natural frequencies that are a function of their length and wave velocity. As an AE burst is made up of numerous waves of different frequencies, resonance can be expected. Another interesting effect of dispersion is that higher order resonant modes are no longer integer multiples of the fundamental frequency. This can complicate identification of these artefacts.

In traditional AE processing, various AE parameters are used for describing AE signals. AE energy is calculated by integrating the signal over time. Amplitude and frequency analysis are more meaningful parameters for measuring continuous emissions, whilst count rate and energy analysis are useful for burst emission characterisation [7]. Defining a burst as an event that exceeds a certain threshold, the following features will be extracted and analysed in Part 1 of this study:

Peak amplitude
Burst energy
Duration and/or total counts
Rise time and/or counts to peak
Signal strength.

2. Experimental Method

A variety of short waveguides were tested to illustrate the effects of (a) material properties; (b) length; (c) diameter; (d) face angle and (e) source point on the transmission and reception of pulsed AE bursts.

Forty-eight (48) waveguides were tested in total, fabricated from five materials: Delrin acetal resin (white extruded bar, exact grade unknown), common mild steel (exact grade unknown), SS316, 2024-T3 aluminium and sintered 99.9% alumina ceramic (α-Al_2O_3). Approximate material properties are summarised in Table 1. Sensor face angles were 0˚, 30˚, 45˚ or 60˚; lengths were 30, 43 or 51 mm; and diameters were 5 or 8 mm. Unless otherwise stated, the rod face attached to the pulser was flat.

Test specimens were grouped as follows:

(a) 5 sets of 8-mm diameter waveguides with face angles of 0˚, 30˚, 45˚ and 60˚ from each of the four materials (20 waveguides in total). Lengths were set at 43 mm between centres (at which pulser and receiver were located).
(b) 3 sets of 8-mm diameter, shorter (30 mm) waveguides with face angles of 0˚, 30˚, 45˚ and 60˚; from Delrin, 2024-T3 aluminium and SS316.
(c) 2 sets of narrower (5 mm) mild steel rods, 30mm and 43mm in length, with face angles of 0˚, 30˚, 45˚ and 60˚.
(d) 3 longer (51 mm) rods from Delrin, 2024-T3 aluminium and SS316, 0˚ sensor face angle.
(e) 5 8-mm diameter, 43-mm long rods from mild steel (1 of), SS316 (1 of) or AL2024-T3 (3 of), each with one end tapered (45˚) to a point (pulser end). The sensor end was always flat.

More specifically the details of each were:

- 1 x MS waveguide with dull point
- 1 x SS316 waveguide with sharp point
- 1 x AL2024-T3 waveguide with a flat point (1.6 mm in diameter)
- 1 x AL2024-T3 waveguide with dull point
- 1 x AL2024-T3 waveguide with sharp point

The following designation is used to describe samples:

Material x *Diameter in mm* x *Nominal Length in mm* "*PT*" (optional).

To quantify the effect of each waveguide, data was also collected from the sensor mounted directly on the pulser face. The resulting values were used to normalise all data.

Table 1: Approximate acoustic properties of test materials used in theoretical calculations.
* Properties given for Delrin [9].

Material	Abbreviation	Density (g/cm^3)	c_L (mm/μs)	c_T (mm/μs)	Z_L
Delrin *	DR	1.42	1.8	0.9	2.6
Mild Steel	MS	8.00	5.6	3.1	45
SS316	SS	7.89	5.7	3.0	45
AL2024-T3	AL	2.77	6.4	3.1	17.7
α-Al_2O_3	ALM	3.9	10.6	3.5	40.6

Longitudinal pulses, representative of AE bursts, were generated by a DECI Model SE25-P sensor driven by a DECI Model 600 pulser, set at 150V. A waveguide holder (Fig. 3) was fabricated to ensure that the relative positions of the sensor, waveguide and pulser were kept constant. The pulser was attached to the underside of the holder with a Delrin collar containing 8 rare earth magnets and two locating pins to ensure repeatable orientation. Incorporated into the sensor mount was a screw and spring that held the sensor firmly against the top waveguide face. This could be oriented to any angle. O-rings prevented the waveguides from contacting the sides of the sample holder. Silicone grease was used as a couplant between the pulser-waveguide and waveguide-sensor faces.

Bursts were detected using a B1080 Digital Wave Corp. single-ended wideband AE sensor connected to a PAC 2/4/6 preamplifier supplying a gain of 20 dB and fitted with 100-1000 kHz bandpass filters. Data was recorded with a PAC PCI-2 card, which was housed in a 2.8-GHz Pentium-IV desktop computer. Prior to digitisation, signals were bandpass filtered onboard at 1-3000 kHz. A fixed trigger threshold was set at 50 dB_{AE}. For each waveguide, between 128 and 300 triggered waveforms, each consisting of 8192 samples with 256 pre-trigger samples, were collected and digitised at 10 MHz.

Various burst features were collected using PAC's AEWin software for each triggered event, including peak amplitude (in dB_{AE}), AE energy, signal strength, duration, rise time and AE counts. These were then averaged and graphed. All values used in any particular average varied by less than 2% indicating high pulser repeatability. Individual waveforms were also captured and averaged to remove the effects of random instrumentation noise.

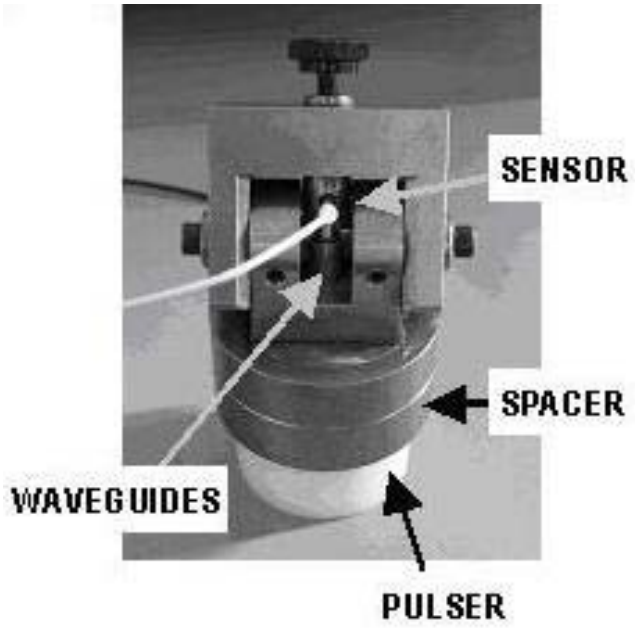

Fig. 3 Waveguide holder.

3. Results and Observations

3.1 Burst profiles

As can be seen clearly in Fig. 4, waveform profiles being received by the sensor vary significantly between materials. Alumina ceramic appears by first inspection most like the face-to-face signal but greatly reduced in amplitude. On the other hand, waveforms associated with both steels are significantly protracted and full of broadband artefacts. Aluminium wavefront also

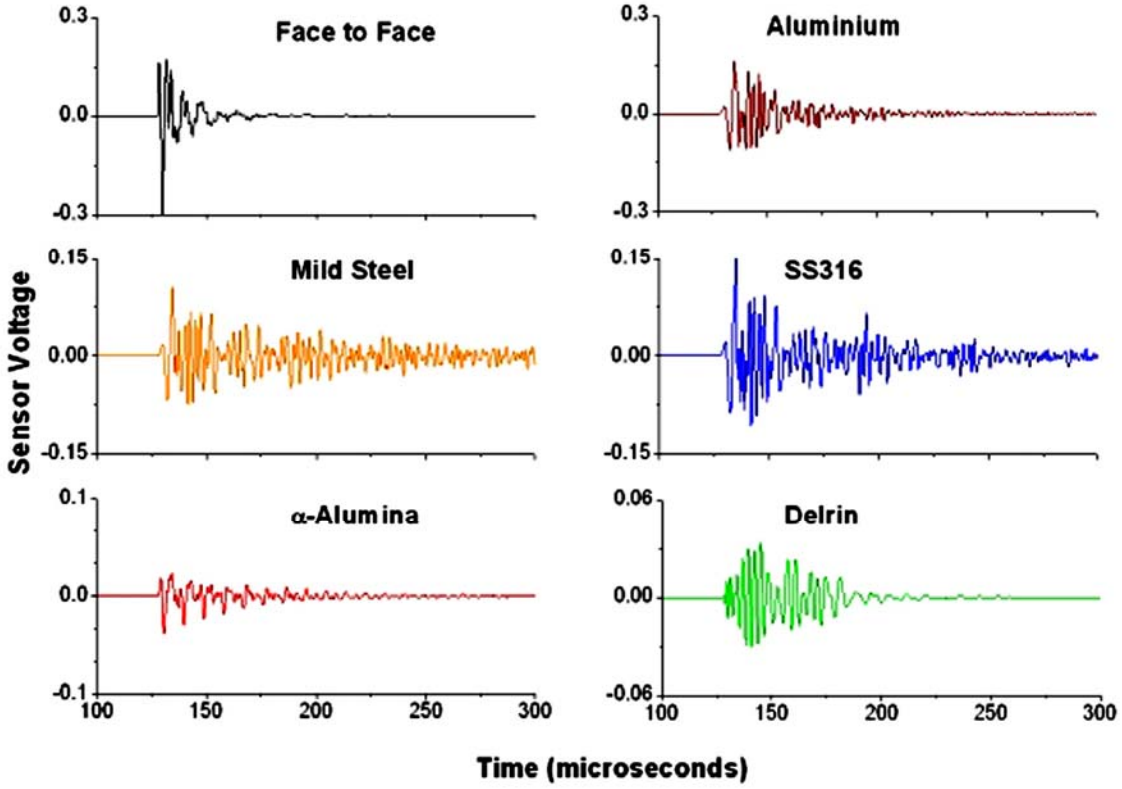

Fig. 4 Time waveforms for flat waveguide samples. Different y-scales are used to facilitate better appreciation of waveform profiles. Time scales are identical.

appears filled with similar broadband artefacts. This loss of waveform fidelity was also observed by Ono, in his tests on longer samples of the same material using lasers as a source of AE [10]. Mode separation is most obvious in the Delrin sample, which has also lost the pulse's sharp wavefront.

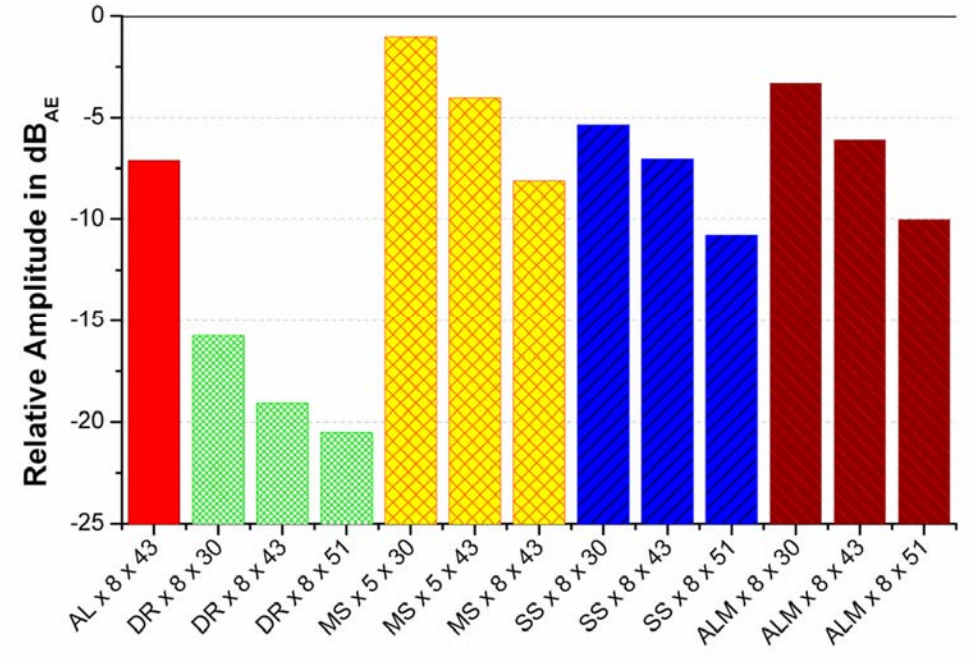

Fig. 5 Amplitude for different flat-faced waveguides.

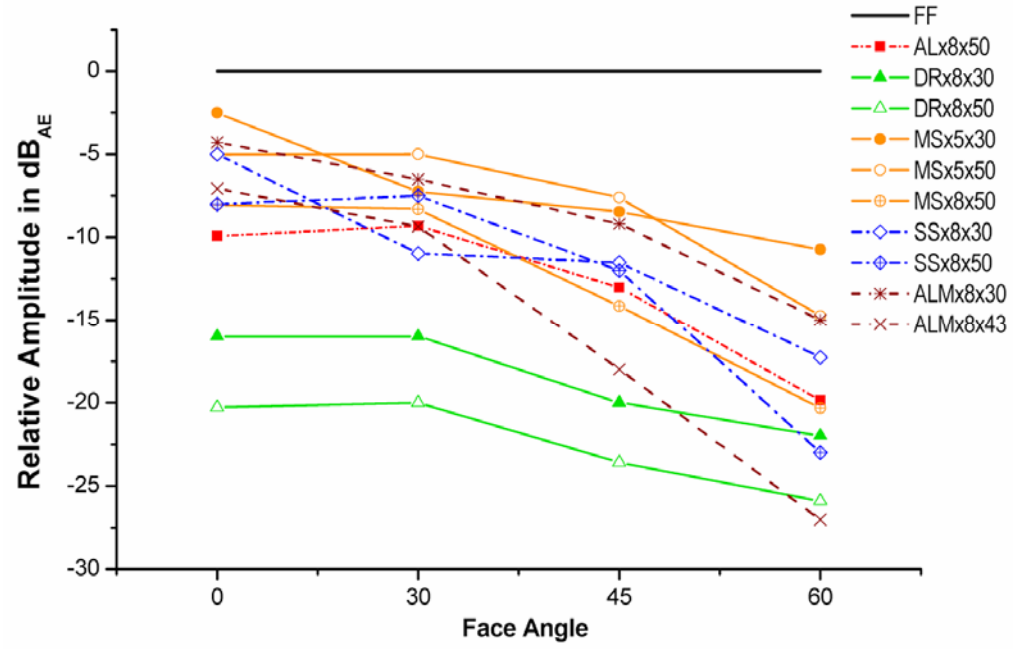

Fig. 6 Amplitude versus face angle for all sets of angled samples.

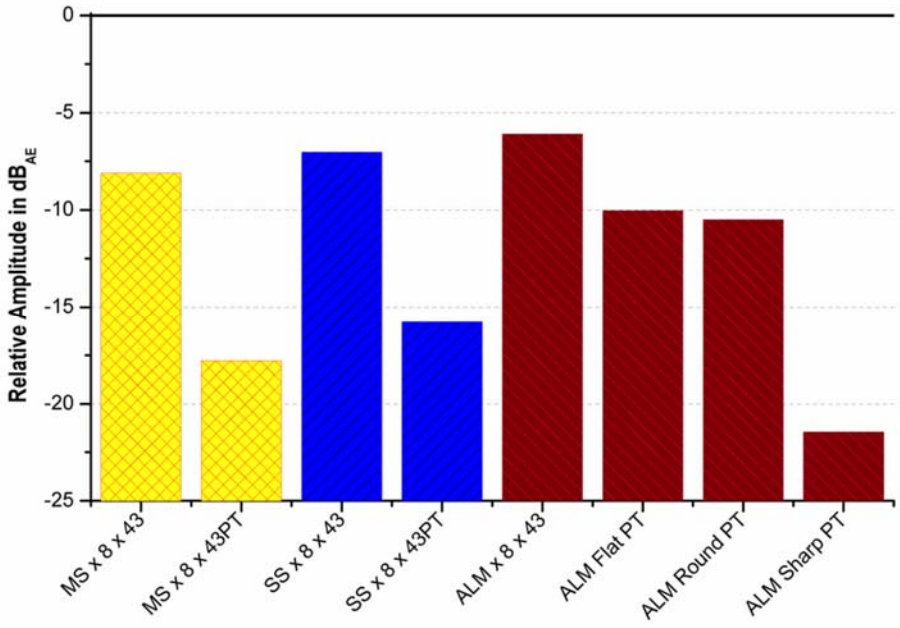

Fig. 7 Effect on amplitude by using a pointed waveguide**.**

3.2 Amplitude and energy

The effects on amplitude were very similar for most waveguides as can be seen from Figs. 5 to 7. The trend for energy was similar. These show that both parameters decreased with length, increased diameter and increased face angle. As expected, attenuation was higher for α-Al_2O_3 and Delrin. For the three materials from which different length waveguides were tested, approximate values for attenuation were calculated (see a table below).

Although these numbers are very approximate, they do indicate that Delrin's broadband attenuation is highly non-linear and in this application (across the frequency range studied) significantly less than predicted by the literature.

	Average peak amplitudes of samples in dB_{AE}			Attenuation
	30 mm	51 mm	Difference	dB/m
SS316	107.7	101.0	6.7	319
AL2024-T3	105.6	100.2	5.4	257
Delrin	95.3	90.5	4.8	229

3.3 Rise time, duration and counts

Rise-times (and counts to peak) were greatest for Delrin, due to its much lower speed, and obvious mode separation. Otherwise material effects on rise-time were minimal. There were also no clear relationships between length, face angle and rise-time. The same cannot be said for pointed waveguides, as shown in Fig. 8, which caused rise-times to increase significantly in all three materials tested.

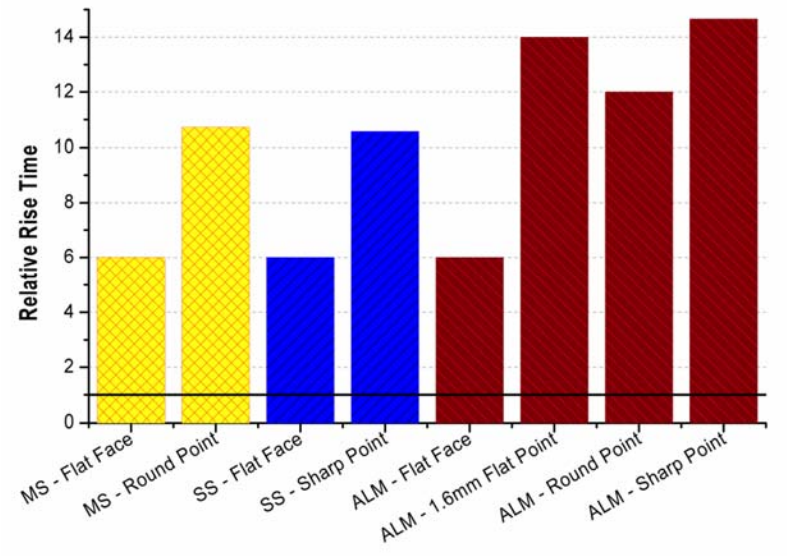

Fig. 8 Effect of pointed end on rise-times.

Durations (and AE counts) were affected by material properties, as shown in Fig. 9. Results support initial observations from time waveforms, with steel samples showing the highest durations, which increased with both length and diameter.

However, results for other materials were less consistent. Although alumina appeared to have a very similar waveform to the originating pulser burst, its much smaller duration value suggests that its calculation is as much a feature of the fixed threshold value as it is the waveform profile: a small signal takes less time to drop below the fixed 50 dB_{AE} trigger level. (A smaller threshold, closer to the true noise floor, may have lessened this affect.)Neither face angles, nor end points had any appreciable effect on durations.

4. Discussion

4.1 Effect of material

Little difference in the time domain can be seen between mild steel and stainless steel waveguide responses, especially when compared to other material samples. AE features analysed were also consistent between the two steel grades, indicating that neither material has any obvious

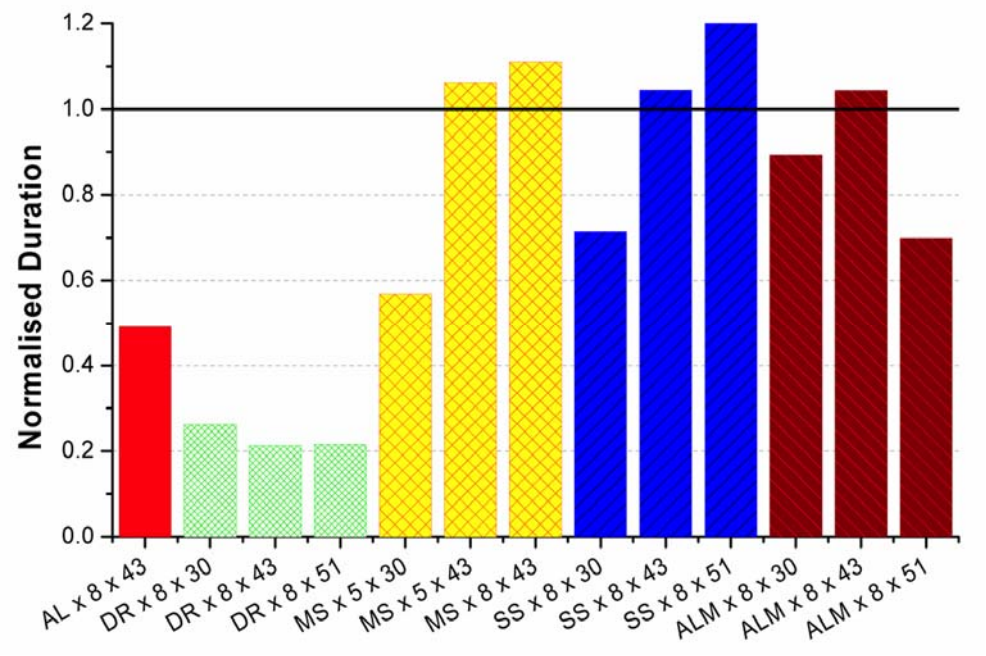

Fig. 9 Material effects on duration.

acoustic superiority over the other. Durations and counts were substantially higher in both grades of steel and both features increased with rod length. The reason for this is not immediately obvious from the tests in this paper but is the subject of investigations presented in Part 2.

Of the metallic specimens, 2024-T3 aluminium samples transmitted pulses with the least signal distortion. However waveforms still appeared protracted and filled with broadband artefacts not present in the original signal, although not as much as in either steel. Alumina ceramic was the least distorted of all materials, with signals appearing similar to the originating bursts. Delrin, due to its much slower wave speed, showed the clearest mode separation of all materials.

As predicted, overall attenuation of both energy and peak amplitude was greatest in non-metallic waveguides, however rudimentary calculations based on drop in peak amplitude for different lengths indicated that this was not as severe as was expected. Furthermore, any attenuation present in Delrin seemed to be non-linear and therefore longer waveguides caused proportionally less attenuation than shorter guides across the traditional AE bandwidth.

4.2 Effect of length, diameter and face angle

Attenuation also increased with length and diameter (where measured). Reasons for the latter are not clear, and were only tested for one material (mild steel) but may be due to the increased number of modes present in wider rods (below cutoff). This will be discussed further in Part 2. In all materials, attenuation increased significantly with face angle, particularly above 30 degrees. This is probably because mode conversion is causing redirection of energy into modes that the transducer is less able to detect.

4.3 Effect of pointed source end

Pointed 43-mm waveguides attenuated the signals by over 12 dB when compared to similar flat waveguides with adequate couplant. This was greater than the attenuation quoted by other researchers [10, 11]. The type of point also made a significant difference on amplitude and energy attenuation with finer (sharper) points causing greater signal reduction than rounder or flat

points. This may allude to the discrepancy between these values and those published in other work.

5. Conclusions

Although signals passing through metallic waveguides were not attenuated significantly, signals were protracted and appeared as if contaminated by reflections and resonance artefacts. Conditions deteriorated with length and diameter. It is possible that much longer waveguides (>100mm) might avoid this problem due to the additional attenuation that would be incurred; however this requires further verification. On the other hand, α-Al_2O_3 did not suffer from this problem, with primary bursts being easily separated from subsequent reflections. Although alumina had a higher overall attenuation, measured bursts showed significantly less distortion and (except for amplitude and energy due to its increased attenuation) best-matched AE features of face-to-face signals.

Unfortunately, use of waveguides in AE testing cannot be avoided, however their implementation must be properly considered. Whenever feasible, specific designs should be tested prior to installation to determine actual transmission characteristics.

Further effects on transmission of modal information will be investigated in Part 2.

Acknowledgements

The authors thank IMES Group for supplying the PCI-2 board and software used for data acquisition.

References

1. Graff, K.F. (1975) *Wave motion in elastic solids*, London: Oxford University Press.
2. Redwood, M. (1960) *Mechanical Waveguides*, London: Pergamon Press.
3. Meeker, T.R. and Meitzler (1964) *Guided wave propagation in elongated cylinders and plates, Physical Acoustics*, **1**(A): pp. 112-169.
4. Pao, Y.-H. and Mindlin, R.D. (1960) Dispersion of Flexural Waves in an Elastic, Circular Cylinder, Journal of Applied Mechanics - Trans. ASME, **27**(9): pp. 513-520.
5. Cheeke, J.D.N. (2002) *Fundamentals and Applications of Ultrasonic Waves*, Boca Raton, Florida: CRC Press.
6. Onoe, M., McNiven, H.D. and Mindlin, R.D. (1962) Dispersion of Axially Symmetric Waves in Elastic Rods, Journal of Applied Mechanics - Trans. ASME, **29**(12): pp. 729-734.
7. Raj, B. and Jha, B.B. (1994) Fundamentals of acoustic emission, British Journal of NDT, **36**(1): pp. 16-23.
8. Holroyd, T. (2000) *Acoustic Emission & Ultrasonics*, Oxford, UK: Coxmoor Publishing Co.
9. Dupont *Delrin Design Guide - Module III* [online], Ed. Available from: http://plastics.dupont.com/plastics/pdflit/americas/delrin/230323c.pdf [Accessed 15.03.2004].
10. Ono, K. and Cho, H.-J., (2004) 'Rods and Tubes as AE Waveguides' in *Proceedings of the 26th European Conference on Acoustic Emission Testing*, Berlin: DGZfP, pp. 593-603.
11. Wood, B.R.A., Flynn, T.C., Harris, R.W. and Noyes, L.M. (1991) The use of waveguides in acoustic emission monitoring projects, Acoustics Australia, **19**(3): pp. 87-89.